ELSEVIER

Journal of Power Sources 111 (2002) 152–159

JOURNAL OF POWER SOURCES

www.elsevier.com/locate/jpowsour

Mechanisms of impedance rise in high-power, lithium-ion cells☆

Ira Bloom[a,*], Scott A. Jones[a], Edward G. Polzin[a], Vincent S. Battaglia[a], Gary L. Henriksen[a], Chester G. Motloch[b], Randy B. Wright[b], Rudolph G. Jungst[c], Herbert L. Case[c], Daniel H. Doughty[c]

[a]*Electrochemical Technology Program, Argonne National Laboratory, 9700 South Cass Avenue, Argonne, IL 60439-4837, USA*
[b]*Idaho National Engineering and Environmental Laboratory, P.O. Box 1625, Idaho Falls, ID 83415, USA*
[c]*Sandia National Laboratories, P.O. Box 5800, Albuquerque, NM 87185, USA*

Received 4 May 2002; accepted 14 May 2002

Abstract

Cells were life-cycled cells using profiles with a 3, 6, or 9% change in state of charge (ΔSOC) at 40, 50, 60, and 70 °C. From the voltage response of the cells to the life-cycle profile at each temperature, we separated the overall impedance rise into two simpler terms, R_o (ohmic) and R_p (polarization), using an equivalent circuit model. The R_o data tend to follow the expected trends (40 > 50 > 60 > 70 °C). Although the R_p data trends show that R_p can either decrease or increase asymptotically with time, the overall temperature-dependent behavior is similar to that of R_o. We illustrate the types of processes that can occur in one lithium-ion cell chemistry. Based on the initial rates, the processes are complex. The R_o term dominates the observable cell impedance, but R_p adds a non-trivial contribution.

Keywords: High-power; Impedance; Lithium-ion

1. Introduction

Since their introduction in 1991 [1], Li-ion batteries have found uses in many consumer electronic applications. The batteries generally consist of a metal oxide cathode, a liquid organic solvent containing a dissolved ionic salt, and a carbon-based anode. The US Department of Energy—supported Partnership for the New Generation of Vehicles (PNGV) and others have been evaluating this class of batteries for use in hybrid-electric vehicles. For this application, the batteries must have a useful life of 15 years. However, during their lives, these cells exhibit an impedance increase. Thus, a 15-year life remains a challenge.

Three national laboratories, Argonne National Laboratory (ANL), Idaho National Engineering and Environmental Laboratory (INEEL), and Sandia National Laboratories (SNL), collaborated to evaluate and understand, among other phenomena, the causes of the impedance rise in these cells. A number of 18650-sized cells containing a commercially available chemistry were subjected to accelerated cycle and calendar life testing in this study. The papers describing this study and some of the results appear elsewhere [2,3]. These studies showed that the discharge impedance increase is proportional to $(\text{time})^{1/2}$, regardless of the aging test. The authors infer that the most likely source of this impedance increase is the growth of a solid electrolyte interface (SEI) layer on the surface of one or both of the electrodes.

The PNGV Battery Test Manual [4] describes a simple model to estimate the Ohmic and polarization impedances that constitute the observable discharge and regeneration (regen) resistances. The Lumped-Parameter Model (LPM) [5] attempts to linearize the behavior and response of a battery during a simple, repeatable current profile such as that used in the hybrid pulse power characterization test [4]. The life-cycle profiles used in this study were based on

☆The submitted issue has been created by the University of Chicago as Operator of Argonne National Laboratory (“rgonne”) under Contract no. W-31-109-ENG-38 with the US Department of Energy. The US Government retains for itself, and others acting on its behalf, a paid-up, non-exclusive, irrevocable worldwide license in said article to reproduce, prepare derivative works, distribute copies to the public, and perform publicly and display publicly, by or on behalf of the Government.

*Corresponding author. Tel.: +1-630-252-4516; fax: +1-630-252-4176.
E-mail address: bloom@cmt.anl.gov (I. Bloom).

0378-7753/02/$ – see front matter
PII: S0378-7753(02)00302-6

current, not power, so the LPM was used to analyze the life-cycle voltage and current versus time data. From this analysis, we show that the underlying mechanisms are sensitive to the state of charge (SOC), amount of charge removed during the cycling (ΔSOC), and the temperature.

2. Experimental

Details of the cell chemistry and the conditions that the cells were exposed to are given in [2]. Briefly, 135 0.9 A h, 18650-sized cells were built to ANL specifications. The cells consisted of a $Li(Co_{0.2}Ni_{0.8})O_2$ plus SFG-6 + carbon black graphite cathode, 1 M LiPF6 in EC:DEC (1:1 by wt) electrolyte, a Celgard separator, and a MCMB-6 + SFG-6 graphite anode. The active area was 678 cm^2. The cycle-life cells were aged at 60 and 80% SOC at 40, 50, 60, and 70 °C. The cells were cycled using three profiles, 3, 6, and 9% ΔSOC, as shown in Fig. 1. Three to six cells were exposed to all aging conditions. Every 4 weeks (2 weeks at 70 °C), the cells were cooled to 25 °C to conduct reference performance tests. During the life-cycle experiments, data from every 100th profile were collected at high rates (ca. 10 samples/s). These data were extracted and analyzed in terms of the LPM.

The equivalent circuit used in the LPM is given in Fig. 2a, where OCV is the ideal open circuit voltage; R_o is the internal resistance due to ohmic, interfacial, and kinetic impedances in the cell; R_p is the concentration polarization of the electrolyte and electrodes; C is a capacitance included to simulate the time constant during the polarization of the electrolyte and electrodes; I_L is the load current; $I_p(t)$ the current through the polarization resistance; V_L load voltage; R_L load resistance; t the time; and 1/OCV′ is related to the changes in the diffusion coefficient of Li^+ in the electrodes with time.

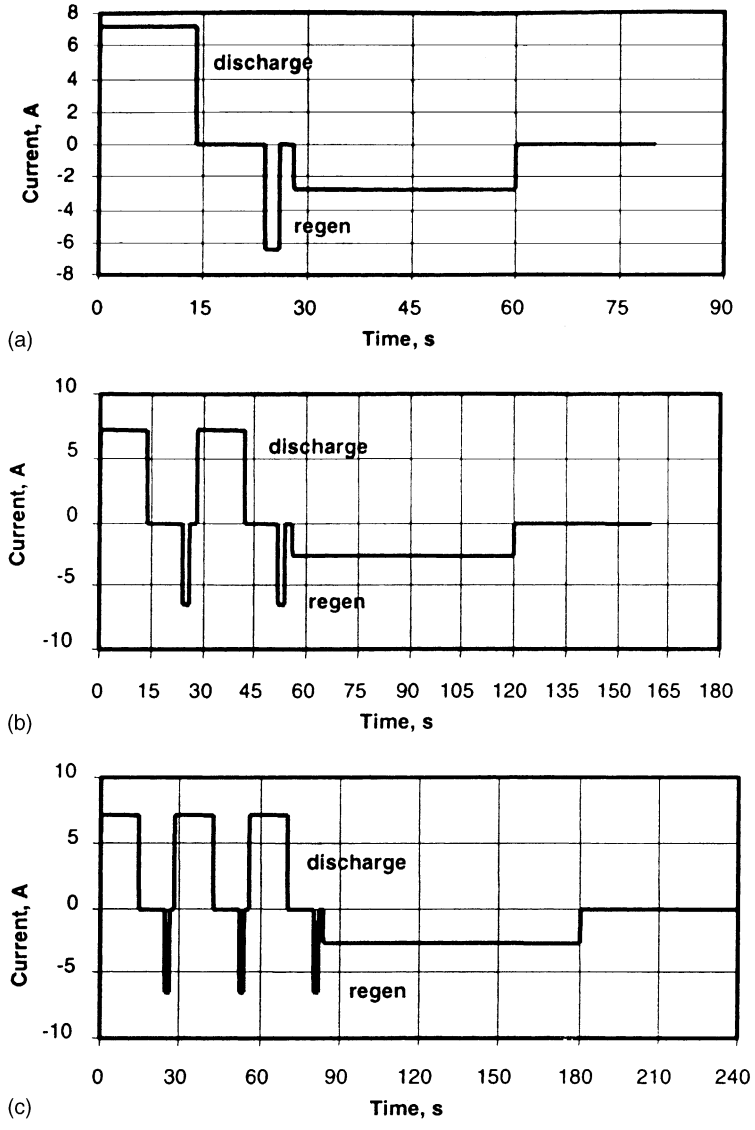

Fig. 1. Cycle-life profiles used: (a) 3% ΔSOC, (b) 6% ΔSOC, (c) 9% ΔSOC.

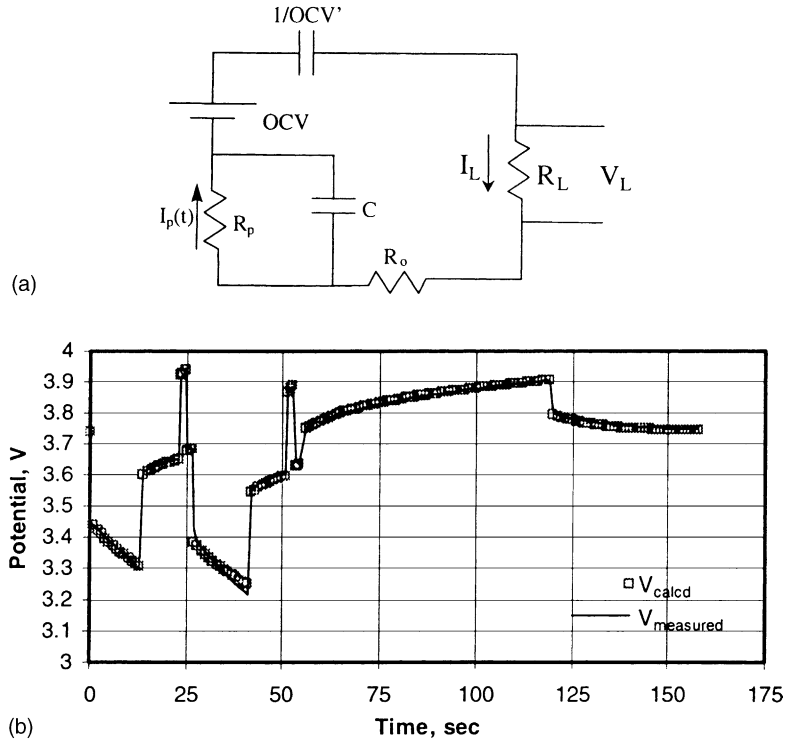

Fig. 2. (a) Equivalent circuit used for the lumped-parameter battery model; (b) comparison of calculated and measured cell voltages.

The relationship between V_L and most of the parameters listed is described by Eq. (1):

$$V_L = \mathrm{OCV} - \mathrm{OCV}'\left[\int I_L \, dt\right] - R_o[I_L] - R_p[I_p] \quad (1)$$

The parameters, OCV, OCV′, R_p, R_o, and τ were calculated by using the linear regression function (LINEST) in Microsoft Excel. An iterative computer algorithm of successive approximations ($\tau + \Delta\tau$) was written to estimate τ (the initial value of $\Delta\tau$ was 1). In this method, the values of successive regression coefficients, r^2, were monitored as a function of τ. As long as r^2 increased, the value of $\Delta\tau$ was not changed and was added to τ. When r^2 decreased, the value of $\Delta\tau$ was halved and negated. This process was continued until two successive values of r^2 did not differ by more than 10^{-10}. Typically, the final values of r^2 were 0.95 or better. Fig. 2b shows that the calculated values agree well with the measured cell voltage values.

After the calculations were completed, the individual values of R_o and R_p were averaged. The time-dependencies of R_p and R_o were determined by curve fitting. The type of equation used is given in Eq. (2):

$$Q = f(t), \quad (2)$$

where $Q = R_o$ or R_p, and $f(t)$ is of the form $at + b$, $a\ln(t) + b$, $at^{1/2} + b$, $at^{1/2} + b\ln(t) + c$ (a, b, c = constants, t = cycle count), or some linear combination of them. The form of the equation was selected based on its value of r^2 resulting from fits of the data. The form of Q was altered while monitoring r^2; if a more complex form of the function yielded a significantly higher r^2 (e.g. 0.85 versus 0.95), then the new function was selected as the one more representative of the process.

3. Results and discussions

An abbreviation system is used below to denote the experimental conditions. It signifies the SOC, ΔSOC, and temperature of the experiment. For example, "80360" signifies 80% SOC, 3% ΔSOC at 60 °C, and 60940 signifies 60% SOC, 9% ΔSOC at 40 °C. If the temperature field is denoted as "XX," then we are referring to the entire group of cells at a particular SOC and ΔSOC. It should be noted that data from the first ~5000 cycles or the first 4-week soak interval (2 weeks at 70 °C) were used (approximately 10,000–25,000 cycles). After that, the data were either obscured by experimental artifacts or too complex to rationalize. Hence, the analyses indicate the initial mechanisms and rates only. For clarity, the remaining discussion is divided according to source of the impedance, R_o or R_p.

3.1. Ohmic impedance rise (R_o)

Typical plots of R_o versus cycle count for cells cycled at 60% SOC are given in Fig. 3; plots for those cycled at 80% SOC, in Fig. 4. Comparison of Figs. 3 and 4 shows both similarities and differences. The general shapes of R_o versus

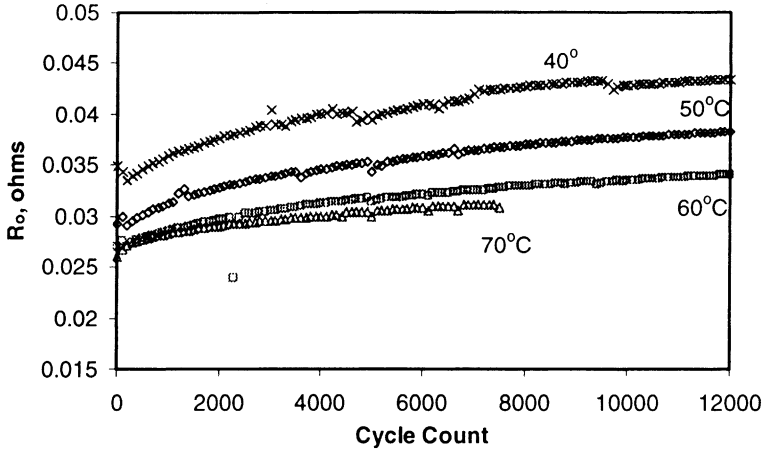

Fig. 3. Average R_o vs. cycle count for cells at 606XX (XX = temperature given on plot).

cycle count are similar, but their dependence on temperature is different. In Fig. 3, the 60% SOC data follow a simple, temperature-dependent trend. The values of R_o decrease with rising temperature, $40 > 50 > 60 > 70$ °C. However, Fig. 4 shows that this is not the case at 80% SOC. The values of R_o decrease as $40 > 50 > 70 > 60$ °C. Exactly, why the 80% SOC values do not follow the expected trend is not known.

The values of the coefficients of the fitting equation, $a\ln(t) + bt^{1/2} + c$, and the values of r^2 from curve fitting, are given in Table 1 for cells aged at 60% SOC. The corresponding data from the 80% SOC cells using the equation $at^{1/2} + b$ are given in Table 2. As can be seen from the high values of r^2, the fits are very good. A plot showing typical the agreement between the data and the fits is given in Fig. 5.

From Tables 1 and 2, we can see that the form of the equation that describes R_o differs according to SOC; the form of the equation for 60% SOC differs from that for 80% SOC. Though the values of the coefficients can be used to compare absolute rates, the form of the equation reveals much about the underlying processes.

Square-root-of-time-dependent (parabolic kinetics), as well as logarithmic-with-time, mechanisms have been found for the growth of an oxide film on a metal surface [6–14]. The square-root-of-time-dependent mechanism tends to have a strong thermal diffusion component, tends to follow Arrhenius-like kinetics, and results in the formation of compact scales. In the logarithmic-with-time case, the rate of oxidation starts rapidly and soon becomes slow. This rate law has been described as following from either the absorption of reactive species or the effect of electric fields in or across the oxide layer.

Applying this analogy to the Li-ion battery case, R_o behaves as though the formation of a thin film or some other resistive layer on a battery electrode may occur in much the same manner as an oxide film on a metal. In the 60% SOC case, the form of the equation implies that the reaction starts very quickly and then slows down. The initial reaction between the electrolyte and electrode(s) may involve absorption of the organic electrolyte and/or LiPF6 on the electrode surface as the rate-determining step. The absorbed material then reacts quickly to form a very thin layer. As soon as sufficient material has reacted—hence, the

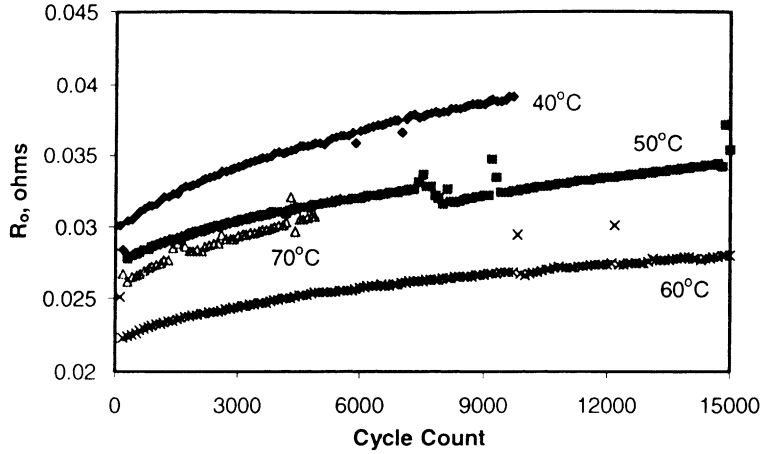

Fig. 4. Average R_o vs. cycle count for cells at 803XX (XX = temperature given on plot).

Table 1
Coefficients for R_o vs. cycle count equations for 60% SOC

SOC (%)	Temperature (°C)	ln(t)	$t^{1/2}$	Constant	r^2
3	40	5.84×10^{-5}	5.86×10^{-5}	2.46×10^{-2}	0.97
	50	3.77×10^{-4}	4.69×10^{-4}	2.07×10^{-2}	0.98
	60	4.95×10^{-4}	2.24×10^{-5}	1.77×10^{-2}	0.91
	70	-2.01×10^{-4}	4.16×10^{-5}	2.26×10^{-2}	0.97
6	40	1.50×10^{-3}	4.98×10^{-5}	2.41×10^{-2}	0.98
	50	9.24×10^{-4}	5.98×10^{-5}	2.30×10^{-2}	0.99
	60	3.63×10^{-4}	6.16×10^{-5}	2.42×10^{-2}	0.99
	70	2.90×10^{-4}	4.18×10^{-5}	2.50×10^{-2}	0.99
9	40	-6.74×10^{-4}	1.80×10^{-4}	3.24×10^{-2}	0.98
	50	9.87×10^{-5}	9.54×10^{-5}	2.83×10^{-2}	0.98
	60	5.36×10^{-4}	5.93×10^{-5}	2.54×10^{-2}	0.96
	70	3.81×10^{-5}	8.12×10^{-5}	2.52×10^{-2}	0.98

Table 2
Coefficients for R_o vs. cycle count equations for 80% SOC

SOC (%)	Temperature (C)	$t^{1/2}$	Constant	r^2
3	40	1.11×10^{-4}	2.81×10^{-2}	0.99
	50[a]	6.20×10^{-5}	2.69×10^{-2}	0.91
	60	5.69×10^{-5}	2.14×10^{-2}	0.96
	70	9.07×10^{-5}	2.46×10^{-2}	0.92
6	40	1.15×10^{-4}	3.52×10^{-2}	0.96
	50	1.49×10^{-4}	3.17×10^{-2}	0.92
	60	9.11×10^{-5}	2.64×10^{-2}	1.00
	70	1.36×10^{-4}	2.93×10^{-2}	0.91
9	40	2.29×10^{-4}	3.16×10^{-2}	0.91
	50	1.27×10^{-4}	3.12×10^{-2}	0.96
	60	8.20×10^{-5}	2.95×10^{-2}	0.88
	70	1.21×10^{-4}	2.64×10^{-2}	0.95

[a] This condition could also be expressed as $R_o = 1.70 \times 10^{-4} \ln(t) + 1.70 \times 10^{-2}$. The value of r^2 is 0.91.

layer has grown—the reaction slows down. At this point, the diffusion of Li^+ and electrons through the layer become the rate-limiting step. The change in rate-limiting step is reflected by the parabolic term in the equation. Unfortunately, our results do not indicate on which electrode these reactions occur. Reports in the literature indicate that the greatest impedance rise for our cell chemistry occurs on the cathode due to SEI layer growth [12].

From the 80% SOC data, the form of the equation indicates that parabolic kinetics are operating. That is, the diffusion of Li^+ and/or electrons through the film may be the rate-determining step, not the adsorption of materials. Equally possible, the diffusion of electrolyte solvent and/or salt molecules through the film to the cathode could be the rate-determining step.

Conceptually, the anode could also play an important role in the impedance rise. Similar mechanisms as described for the cathode may be operating. Based on the data, we cannot differentiate which electrode contributes the most to the impedance rise.

Plotting the coefficients of the $t^{1/2}$ terms on Arrhenius plots yields additional information (Fig. 6). At 60% SOC, Arrhenius kinetics are followed at 3% ΔSOC; at 9% ΔSOC, Arrhenius kinetics are followed up to (and including) 60 °C. Arrhenius kinetics are not followed at 6% ΔSOC ($r^2 = 0.11$). From the slopes of the lines in Fig. 5, the thermal

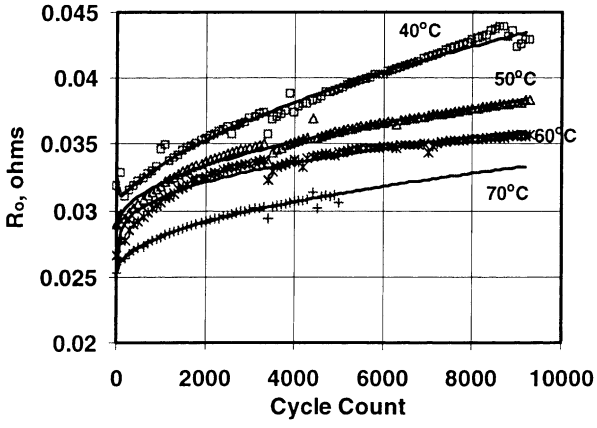

Fig. 5. Average R_o vs. cycle count and fitting curves using the data in Table 1 for 609XX (XX = temperature on graph). The markers represent the values of the average R_o and solid lines represent the fitting curves.

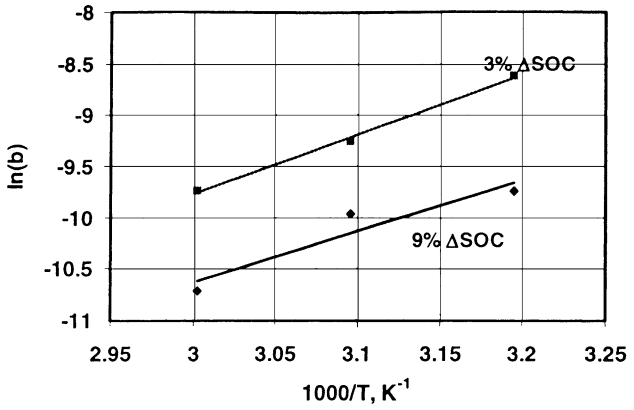

Fig. 6. Arrhenius plot of the coefficients of the $t^{1/2}$ term for 3 and 9% ΔSOC at 60% SOC.

activation energies (E_a) for R_o are 41.3 ± 13.6 ($r^2 = 0.90$) and 48.2 ± 3.2 kJ/mol ($r^2 = 1.00$) for 3 and 9% ΔSOC, respectively. These values are the same within experimental error.

Note that the coefficients of the ln(t) term also follow Arrhenius kinetics. From the slope of the line, the value of E_a is 52.7 ± 8 kJ/mol ($r^2 = 0.96$).

The same exercise using the 80% SOC, R_o data shows that only 9% ΔSOC seems to follow Arrhenius kinetics, and then only up to 60 °C. Here, the value of E_a for R_o is 44.6 ± 3.0 kJ/mol ($r^2 = 1.00$). There is no significant difference between this and the previous values of E_a.

3.2. Polarization impedance rise (R_p)

Typical plots of R_p versus cycle count are given in Figs. 7 and 8 for cells cycled at 60 and 80% SOC, respectively. Comparing Figs. 7 and 8 shows two very different behaviors in R_p. In Fig. 7, the value of R_p decreases asymptotically with cycle count; in Fig. 8, there is a slow increase. It is clear that the curves in Fig. 7 follow an expected trend based on temperature, $40 > 50 > 60 > 70$ °C. In Fig. 8, this is not the case.

The values of the coefficient, the form of the equation, and the values of r^2 from the curve fitting are given in Table 3 for cells aged at 60% SOC. As explained below, there are two rows of coefficients for the 606XX conditions, one for an equilibration process and the other for a degradation process. The corresponding data from the 80% SOC cells are given in Table 4. As can be seen from the high values of r^2, the fits are very good, with two exceptions. The data from 60340 seem constant with cycle count, and the data at 80940 show too much scatter.

From the data in Table 3, the 60340 data indicate that there is no dependence of R_p on cycle count. This implies that there is little, if any, change in concentration polarization in the cells. As the temperature increases, the amount of concentration polarization increases, most likely due to higher reaction rates for the decomposition of electrolyte at the higher temperatures.

The R_p data for 603XX are given in Fig. 9. On the basis of their shapes, together with the positive coefficients in Table 3, these curves may be indicative of a system that is mass-transport limited, causing the concentration polarization to increase according to some simple function of cycle count.

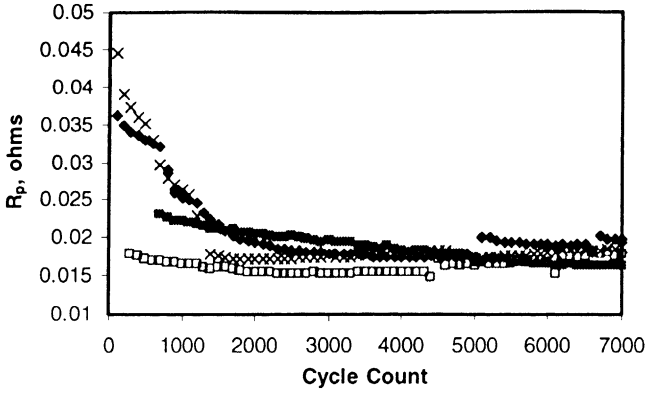

Fig. 7. R_p vs. cycle count for 606XX (XX = temperature on graph).

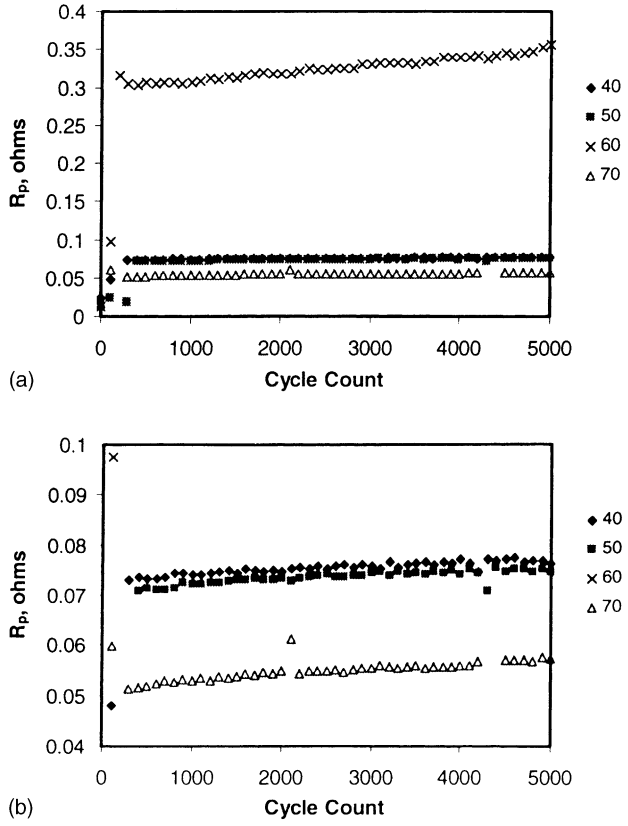

Fig. 8. (a) R_p vs. cycle count for 803XX (XX = temperature on graph); (b) enlargement of a section of Fig. 8a to show the detail.

The situation is more complex at 606XX. The curves in Fig. 7 seem to asymptotically reach a constant value. We found that the R_p data could be expressed as an equilibration process plus a degradation reaction. This is shown in Table 3 by means of two rows of coefficients for each temperature. The upper row with the negative coefficient is the equilibration process and the bottom, the degradation. The degradation rate constants were calculated by subtracting the best-fit curve from the R_p data. Fig. 10 shows a typical plot of the R_p data, the equilibration process, and the degradation reaction. It is interesting to note that all the equilibration processes follow $t^{1/2}$ kinetics, as do most of the degradation reactions. As indicated by the $t^{1/2}$ time dependence, they seem to be diffusion-limited.

The remaining data from 60% SOC (609XX) and most of the 80% SOC follow the same basic trend with cycle count. The rate constants are positive, indicating that the concentration polarization increases with time. The 80960 data indicate that an equilibrium process may be occurring; the rate constant is negative. However, we could not deduce the degradation rate equation with any degree of confidence.

Table 3
Coefficients for R_p vs. cycle count equations for 60% SOC

SOC (%)	Temperature (°C)	t	ln(t)	$t^{1/2}$	Constant	r^2
3	40	None	None	None	4.18×10^{-1}[a]	
	50		7.71×10^{-3}		3.00×10^{-1}	0.90
	60		3.37×10^{-4}		2.92×10^{-1}	0.93
	70	1.76×10^{-6}			2.83×10^{-1}	0.91
6	40			-8.31×10^{-4}	5.23×10^{-2}	0.98
		8.48×10^{-6}			-1.58×10^{-2}	1.00
	50			-5.27×10^{-4}	4.32×10^{-2}	0.96
				3.86×10^{-4}	-1.68×10^{-2}	0.95
	60			-1.16×10^{-4}	2.58×10^{-2}	0.99
				1.17×10^{-4}	-9.50×10^{-3}	0.99
	70			-7.29×10^{-5}	1.89×10^{-2}	0.97
				1.73×10^{-4}	-9.50×10^{-3}	0.93
99	40	9.17×10^{-7}			1.89×10^{-2}	0.93
	50			9.04×10^{-5}	1.57×10^{-2}	0.97
	60			7.41×10^{-5}	1.34×10^{-2}	0.94
	70	3.84×10^{-7}			1.33×10^{-2}	0.96

[a] Considerable scatter in data.

Table 4
Coefficients for R_p vs. time equations for 80% SOC

SOC (%)	Temperature (°C)	ln(t)	$t^{1/2}$	Constant	r^2
3	40	6.50×10^{-4}		3.65×10^{-2}	0.95
	50[a]		7.25×10^{-5}	7.00×10^{-2}	0.91
	60		1.35×10^{-3}	2.58×10^{-1}	0.97
	70		1.03×10^{-4}	4.98×10^{-2}	0.97
6	40		1.13×10^{-3}	-5.37×10^{-1}	0.99
	50		5.08×10^{-1}	-7.84×10^{-2}	1.00
	60		1.76×10^{-4}	2.08×10^{-2}	0.94
	70		8.82×10^{-4}	3.99×10^{-1}	0.98
9	40	No trend obvious due to scatter in data			
	50		2.34×10^{-4}	4.73×10^{-3}	0.99
	60	-3.19×10^{-3}		9.08×10^{-2}	0.93
	70[b]		4.31×10^{-5}	8.09×10^{-3}	0.96

[a] This could also be represented as $R_p = 1.80 \times 10^{-3} \ln(t) + 5.98 \times 10^{-2}$, $r^2 = 0.90$.
[b] This could also be represented as $R_p = 8.38 \times 10^{-4} \ln(t) + 3.74 \times 10^{-3}$, $r^2 = 0.97$.

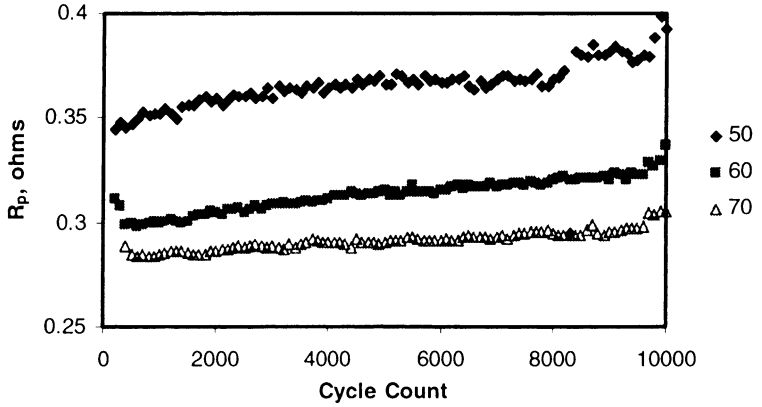

Fig. 9. R_p vs. cycle count for 603XX (XX = temperature), where the 60340 data have been omitted.

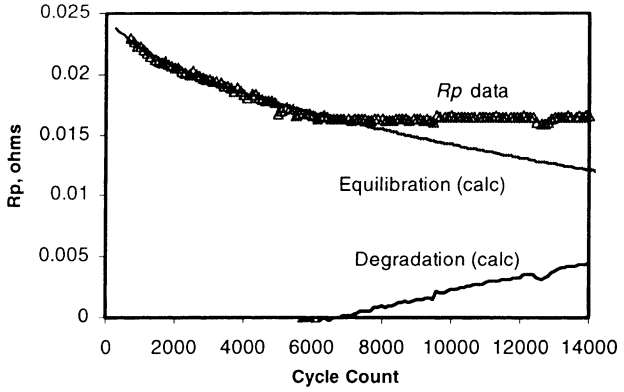

Fig. 10. Plot of R_p vs. cycle count for the data, an equilibration process and a degradation reaction.

4. Conclusions

From the voltage response of the cells to the life-cycle profile at 40, 50, 60, or 70 °C, we have separated the overall impedance rise into two simpler terms, R_o and R_p. The R_o data tend to follow expected temperature-dependent trends ($40 > 50 > 60 > 70$ °C). The R_p data trends show that R_p can either decrease or increase asymptotically with time, but the overall temperature-dependent behavior is similar to that of R_o.

Specifically, at 60% SOC, R_o can be expressed as an equation of the form, $a\ln(t) + bt^{1/2} + c$. This form of the equation implies that there is an initial rapid reaction (e.g. SEI formation) that slows down with time into diffusion-limited kinetics. The coefficients of both the $\ln(t)$ and $t^{1/2}$ terms from the 3 and 6% ΔSOC data display Arrhenius-like behavior. At 80% SOC, the equation for R_o is simpler, $at^{1/2} + b$, with the coefficients of $t^{1/2}$ displaying Arrhenius-like behavior in the temperature range of 40 to 60 °C.

For R_p at 60% SOC, two processes may be occurring: an equilibration and a degradation. The former follows $at + b$ or $at^{1/2} + b$ kinetics, while the latter, follows $at^{1/2} + b$ only. Only the data from 6% ΔSOC displayed clear evidence of the degradation process. At 80% SOC, the equilibration process followed either $a\ln(t) + b$ or $at^{1/2} + b$ kinetics. There was no clear evidence of degradation processes.

We have illustrated the types of processes occurring in one Li-ion cell chemistry. Based on the initial rates, the processes are complex and inter. The R_o term dominates the dependent observable cell impedance, but R_p adds a non-trivial contribution. Together, they describe how the cell performs and how its performance changes with time.

Acknowledgements

Work supported by the US Department of Energy, Office of Advanced Automotive Technologies, Office of Transportation Technologies, under contract W-31-109-ENG-38.

References

[1] O. Kazunori, M. Yokokawa, Cycle performance of lithium ion rechargeable battery, in: Proceedings of the Tenth International Seminar of Primary and Secondary Battery Technology Applications, Deerfield Beach, Florida Educational Seminars, Boca Raton, FL, 1–4 March 1993.
[2] I. Bloom, B.W. Cole, J.J. Sohn, S.A. Jones, E.G. Polzin, V.S. Battaglia, G.L. Henriksen, C. Motloch, R. Richardson, T. Unkelhaeuser, H.L. Case, J. Power Sources 101 (2001) 238–247.
[3] R.B. Wright, C.G. Motloch, J.R. Belt, J.P. Christophersen, C.D. Ho, R.A. Richardson, I. Bloom, S.A. Jones, V.S. Battaglia, G.L. Henriksen, T. Unkelhaeuser, D. Ingersoll, H.L. Case, S.A. Rogers, R.A. Sutula, J. Power Sources, in press.
[4] PNGV Battery Test Manual, Revision 2, DOE/ID-10597, August 1999, or PNGV Battery Test Manual, Revision 3, DOE/ID-10597, January 2000.
[5] PNGV Battery Test Manual, Revision 2, DOE/ID-10597, August 1999, or PNGV Battery Test Manual, Revision 3, DOE/ID-10597, January 2000, Appendix D.
[6] N. Birks, G.H. Meier, Introduction to High Temperature Oxidation of Metals, Edward Arnold, London, 1983.
[7] P. Kofstad, High-temperature Oxidation of Metals, Wiley, New York, 1966.
[8] K. Hauffe, Oxidation of Metals, Plenum Press, New York, 1965.
[9] W. Jost, Diffusion in Solids, Liquids and Gases, 3rd Edition, Academic Press, New York, 1960, Addendum.
[10] J. Crank, The Mathematics of Diffusion, 2nd Edition, Clarendon Press, Oxford, 1975.
[11] P. Kofstad, Nonstoichiometry, Diffusion, and Electrical Conductivity in Binary Metal Oxides, Wiley, New York, 1972.
[12] K. Amine, M.J. Hammond, J. Liu, C. Chen, D.W. Dees, A.N. Jansen, G.L. Henriksen, in: Proceedings of the Tenth International Meeting on Lithium Batteries, Como, Italy, 28 May to 2 June 2000, p. 332.
[13] E. Strauss, D. Golodnitsky, E. Peled, Electrochem. Solid State Lett. 2 (1999) 115–117.
[14] G. Blomgren, J. Power Sources 81/82 (1999) 112–118.